La Niña–like Mean-State Response to Global Warming and Potential Oceanic Roles

TSUBASA KOHYAMA, DENNIS L. HARTMANN, AND DAVID S. BATTISTI

Department of Atmospheric Sciences, University of Washington, Seattle, Washington

(Manuscript received 8 June 2016, in final form 3 February 2017)

ABSTRACT

The majority of the models that participated in phase 5 of the Coupled Model Intercomparison Project global warming experiments warm faster in the eastern equatorial Pacific Ocean than in the west. GFDL-ESM2M is an exception among the state-of-the-art global climate models in that the equatorial Pacific sea surface temperature (SST) in the west warms faster than in the east, and the Walker circulation strengthens in response to warming. This study shows that this "La Niña–like" trend simulated by GFDL-ESM2M could be a physically consistent response to warming, and that the forced response could have been detectable since the late twentieth century. Two additional models are examined: GFDL-ESM2G, which differs from GFDL-ESM2M only in the oceanic components, warms without a clear zonal SST gradient; and HadGEM2-CC exhibits a warming pattern that resembles the multimodel mean. A fundamental observed constraint between the amplitude of El Niño–Southern Oscillation (ENSO) and the mean-state zonal SST gradient is reproduced well by GFDL-ESM2M but not by the other two models, which display substantially weaker ENSO nonlinearity than is observed. Under this constraint, the weakening nonlinear ENSO amplitude in GFDL-ESM2M rectifies the mean state to be La Niña–like. GFDL-ESM2M exhibits more realistic equatorial thermal stratification than GFDL-ESM2G, which appears to be the most important difference for the ENSO nonlinearity. On longer time scales, the weaker polar amplification in GFDL-ESM2M may also explain the origin of the colder equatorial upwelling water, which could in turn weaken the ENSO amplitude.

1. Introduction

The tropical Pacific Ocean has profound impacts on the global climate system, and the response of this region to anthropogenic greenhouse gas forcing has been a controversial research topic since the late twentieth century (e.g., Knutson and Manabe 1995; Cane et al. 1997; Collins et al. 2005; DiNezio et al. 2009; Collins et al. 2010; Xie et al. 2010). The recent multidecadal trends of the zonal sea surface temperature (SST) gradient along the equator and its projection under global warming have received particular attention because of their potential impacts on both the tropical and extratropical weather and climate (e.g., Christensen et al. 2013). The projected influence in relation to the SST warming pattern is not limited to the mean-state land temperature and precipitation changes, but also extends to many other climatological elements, such as frequency of tropical cyclone genesis (e.g., Yokoi and Takayabu 2009; Murakami et al. 2012) and Antarctic sea ice trends (e.g., Kohyama and Hartmann 2016).

In this study, we hereafter call a warming pattern "El Niño–like" ("La Niña–like") when the east (west) equatorial Pacific warms faster than the west (east) equatorial Pacific. Many studies intentionally avoid these terms, which are associated with El Niño–Southern Oscillation (ENSO), because "a reduction in the strength of the equatorial Pacific trade winds is not necessarily accompanied by a reduction in the magnitude of the east–west gradient of SST" as explained by Collins et al. (2010, p. 393). Other studies, however, continue to use ENSO terminology to characterize the structure of global change (e.g., Held et al. 2010; An et al. 2012) presumably because no other simple, lucid way to describe them has been proposed. We have decided to follow the latter, but we shall use these terms carefully in the sense that ENSO is an interannual climate mode that modulates anomalies from the mean state, and that it is not necessarily controlled by the factors that control changes in the mean state under greenhouse warming.

The majority of the models that participated in phases 3 and 5 of the Coupled Model Intercomparison Project

Corresponding author e-mail: Tsubasa Kohyama, kohyama@uw.edu

DOI: 10.1175/JCLI-D-16-0441.1

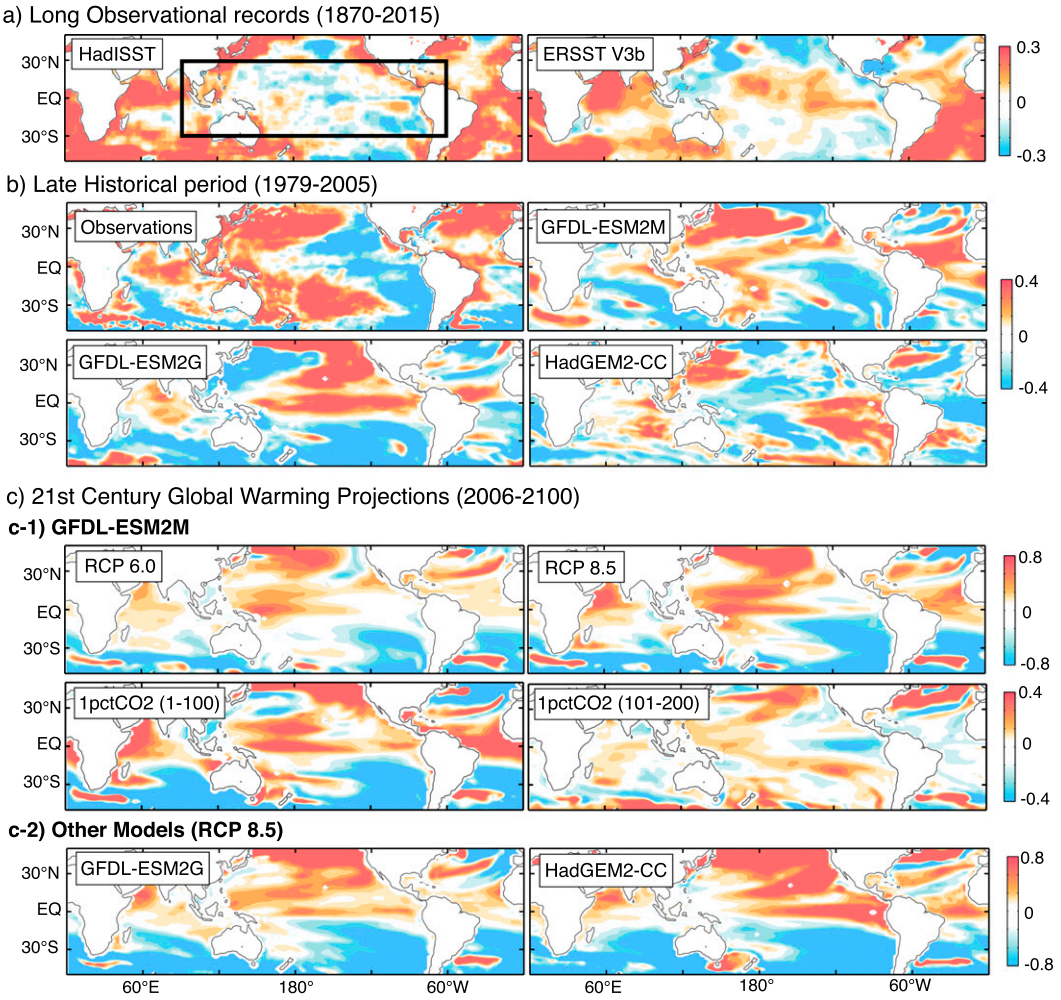

FIG. 1. (a): Observed sea surface temperature (SST) trends computed relative to the tropical Pacific mean trends (30°S–30°N, 90°E–60°W; black box) in two different datasets. Blue colors denote a warming slower than the tropical Pacific mean, not a cooling. Unit is °C $(100\ \text{yr})^{-1}$. (b) As in (a), but for the late historical period. Observations are from the ERA-Interim dataset, and the model output is from the historical runs of GFDL-ESM2M, GFDL-ESM2G, and HadGEM2-CC. Unit is °C $(27\ \text{yr})^{-1}$. (c) As in (a), but for (top) GFDL-ESM2M in the RCP 6.0, RCP 8.5, and 1pctCO2 experiments) and (bottom) GFDL-ESM2G and HadGEM2-CC under RCP 8.5.

(CMIP3 and CMIP5) exhibit El Niño–like SST trends, and therefore, the multimodel mean SST trend pattern is also El Niño–like (e.g., Collins et al. 2010; Huang and Ying 2015; Ying et al. 2016; Zheng et al. 2016). This SST trend pattern has been believed to be associated with the weakening Walker circulation as explained by Held and Soden (2006) and Vecchi and Soden (2007) from the perspective of the global hydrological cycle. In agreement with this, some studies reported that the observed sea level pressure gradient along the equatorial Pacific reduced during the past century (e.g., Vecchi et al. 2006; Zhang and Song 2006; Tokinaga et al. 2012b). Some observational SST datasets support this viewpoint (Fig. 1a, right), although previous studies suggest that the long-term SST trend in the datasets might be sensitive to the time period chosen for analysis (e.g., Meng et al. 2012).

On the contrary, other observational SST datasets suggest that the zonal SST gradient along the equator has increased during the past century (Fig. 1a, left). Some studies based on observed sea level pressure trends (e.g., L'Heureux et al. 2013) and paleoproxies (e.g., An et al. 2012) support this evidence as well. The observational uncertainty of the SST and sea level pressure trends mostly comes from limited data sampling, changing measurement techniques, and different analysis procedures (Christensen et al. 2013). Although we have better datasets based on satellite observations for the late historical period (1979–2005) that also show a clear La Niña–like trend (Fig. 1b, upper left), we

cannot determine, based on the short time span, whether the trend is purely unforced natural multidecadal variability or partly a forced response to anthropogenic climate change. Some model-based studies convincingly show that the fast response to global warming should be La Niña–like and the slow response should be El Niño–like (Held et al. 2010; An et al. 2012; Xiang et al. 2014), but this hypothesis has been difficult to test using observations.

The scientific question we address in this paper is whether a reasonable explanation can be given to support the notion that the forced response of the mean-state equatorial Pacific to greenhouse warming may actually be La Niña–like. Some earlier studies at the end of the last century showed that the global warming trend should be associated with a La Niña–like SST trend because of a so-called ocean dynamical thermostat mechanism (Clement et al. 1996; Cane et al. 1997). This mechanism, however, was simulated by the Cane–Zebiak model (Zebiak and Cane 1987), which assumes that the temperature of the climatological upwelling water in the eastern equatorial Pacific remains fixed as a boundary condition under global warming. This assumption is now thought to be problematic, and after this, La Niña–like SST trends associated with global warming have been largely unexplored using state-of-the-art global climate models (GCMs) or Earth system models (ESMs). This question is still interesting in the sense that, if the warming response is La Niña–like, the recent robust Pacific SST trend during the late historical period (Fig. 1b, upper left) could be understood partly as a forced response rather than purely as multidecadal variability.

In this regard, an interesting member of the CMIP5 model ensemble is the GFDL-ESM2M model (hereafter "M model") in that it produces a well-defined La Niña–like response under historical forcing (Fig. 1b, upper right), the representative concentration pathway (RCP) 6.0 and 8.5 global warming scenarios, and the 1-percent-per-year increase of carbon dioxide (1pctCO2) runs (Fig. 1c). Many studies have shown that the ENSO representation of the M model is reasonable (e.g., Bellenger et al. 2014). The Geophysical Fluid Dynamics Laboratory (GFDL) also developed the GFDL-ESM2G model (hereafter "G model"), which differs from the M model only in its oceanic components (Dunne et al. 2012, 2013), and this model does not exhibit a clear La Niña–like response [Figs. 1b and 1c (bottom)]. Therefore, we hope to identify some important oceanic roles that determine whether the forced response simulated by these models will be El Niño–like or La Niña–like.

In this study, our main focus is to compare the M and G models, and also the HadGEM2-CC model (hereafter "Had model"), which exhibits similar SST trends to the multimodel mean El Niño–like pattern [Fig. 1c (bottom)], to shed light on the possibility of a La Niña–like mean-state warming. Because the late historical period is only about three decades long, the similarity of the SST trends between the observations and the M model could be exaggerated by multidecadal natural variability. Nevertheless, the subtle but detectable resemblance of the SST warming pattern between the historical period (Fig. 1b) and the global warming projections (Fig. 1c) in each of these three models motivates us to hypothesize that the observed SST trend could have already started being forced by global warming during the late historical period. This view may appear to be provocative in the sense that the recent La Niña–like trend has widely been believed to be illustrating the effect of pure natural variability (e.g., Christensen et al. 2013) because of the El Niño–like warming pattern in the majority of the CMIP5 models. It is a hard task to determine whether the M model captures the real world better than other models, but even if its response to warming turns out to be unrealistic, investigating model differences should help us understand the climate system better.

This article is organized as follows. The data used in this study are described in the next section. In section 3, we describe the time evolution of the zonal SST gradient simulated by the three models and associated atmospheric changes to confirm the importance of the differences. Then, in section 4, we show a difference in the capability of the models to simulate a fundamental observed constraint between the zonal SST gradient and the ENSO amplitude in relation to the ENSO nonlinearity. Moreover, by comparing the control, historical, and global warming experiments, we show that the La Niña–like response of the M model is very likely to be forced by global warming. In section 5, we discuss some possible mechanisms whereby the different SST warming responses might be caused by differences of climatology and warming responses in the oceanic interior. A summary and concluding remarks are given in section 6.

2. Data and methods

The observed monthly SST data used in this study are from the Hadley Centre Sea Ice and Sea Surface Temperature (HadISST; Rayner et al. 2003) available online at http://www.metoffice.gov.uk/hadobs/hadisst/index.html and the National Oceanic and Atmospheric Administration (NOAA) Extended Reconstructed Sea Surface Temperature V3b (ERSST V3b; Smith et al. 2008) available online at http://www.esrl.noaa.gov/psd/data/gridded/data.noaa.ersst.html for the time span from 1870 through 2015. The horizontal resolution is 1° for HadISST,

and 2° for ERSST V3b in both the zonal and meridional directions. For the late historical period (1979–2005), we also use the monthly European Centre for Medium-Range Weather Forecasts (ECMWF) ERA-Interim reanalysis data (Dee et al. 2011) available online at http://apps.ecmwf.int/datasets/data/interim-full-moda/levtype=sfc/ for SST (Fig. 1b), zonal wind, and vertical motion (Fig. 3a) with 3° spatial resolution. The starting year of the late historical period (i.e., 1979) is chosen to match the starting year of the ERA-Interim dataset. On the other hand, the ending year of the late historical period (i.e., 2005) is constrained by the CMIP5 experimental design, but the results shown in observations are qualitatively similar even if we extend the time span to be 1979–2015.

The model output of the surface temperature, zonal wind, atmospheric vertical motion, precipitation, oceanic meridional and vertical mass transport, and oceanic potential temperature and density are from the CMIP5 data (Taylor et al. 2012) available at the websites of the GFDL Data Portal (http://nomads.gfdl.noaa.gov:8080/DataPortal/cmip5.jsp) and the Program for Climate Model Diagnosis and Intercomparison (PCMDI; https://pcmdi.llnl.gov/projects/cmip5/). The experiments considered in this study are the first ensemble member of the preindustrial control (piControl), abrupt quadrupling of CO_2 (Abrupt4xCO2), historical, RCP 6.0 and 8.5, and 1pctCO2 runs. At each depth (vertical resolution is 10 m), the oceanic variables are regridded via linear interpolation onto a 2.5° longitude by 2° latitude grid. In addition, we also refer to SST from a 4000-yr-long preindustrial control run of GFDL CM2.1 (Delworth et al. 2006; Wittenberg et al. 2006).

We have also used the RCP concentration calculations and data (Meinshausen et al. 2011) available online at http://www.pik-potsdam.de/~mmalte/rcps/ (to make Fig. 9). The time series used in this study is the RCP 8.5 anthropogenic forcing from 1860 through 2100. Also (to make Fig. 10a), ocean potential temperature data from reanalysis were obtained from the National Centers for Environmental Prediction (NCEP) Global Ocean Data Assimilation System (GODAS) (Behringer and Xue 2004), available online at http://www.esrl.noaa.gov/psd/data/gridded/data.godas.html. The time span used in this study is 1980–2005 (late historical period, but 1979 is not available). The horizontal resolution is 1° longitude by 1/3° latitude, and the vertical resolution is 10 m for the depth analyzed in this study.

Monthly climatologies are calculated by taking the average for each month over the entire record. The climatology is then subtracted from the data to obtain the anomalies unless noted otherwise. All the analysis methods used in this study are simple regression, correlation, and compositing analyses. When we estimate degrees of freedom in the data for statistical tests, we use a formula given by Bretherton et al. (1999) to take autocorrelations into account.

3. SST-warming time evolutions and the Walker circulation changes

Figure 2 shows the spatial patterns of the bidecadal-mean SST (deviations from the global mean) starting from 2016, 2036, 2056, and 2076 expressed with respect to the decadal-mean starting from 2006. Even in the first bidecade, a hint of difference in the zonal SST gradient is already apparent, especially between the M and Had models. Then, after half a century, the three models start to show their distinct spatial structures. The last bidecadal patterns are essentially the same as those introduced in Fig. 1. This temporal evolution confirms that the trend patterns shown in the introduction section are due to a gradual process during this century.

Next, we investigate the trends of the Walker circulation. Figure 3a shows the equatorial meridional-mean trends of zonal wind and vertical motion during the late historical period. During the historical period, both observations and the M model exhibit a strengthening of the Walker circulation. As in the SST trends, however, these trends could be dominated by multidecadal natural variability, so we cannot use this result to demonstrate that the M model is more reasonable than the others. Nevertheless, this correspondence of the signs of these variables motivates us to hypothesize that some portion of these trends might be explained as a response to warming.

Figure 3b shows the same plots as in Fig. 3a, but for the twenty-first-century global warming projections in the three models of interest. The Walker circulation weakens as the SST experiences El Niño–like warming in the Had model, as many previous articles have suggested (e.g., Tokinaga et al. 2012a). By contrast, in the M model, the Walker circulation strengthens as the SST experiences La Niña–like warming. The G model exhibits a weaker signal, particularly in vertical motion, which is consistent with the SST trends without a clear La Niña–like pattern. Although we have no reason to assume that the late historical period is explained by the global warming forcing thus far, the structural resemblance in the Walker circulation change (in particular, the longitudinal correspondence) between the late historical period and the global warming projections by the M model increases the interest in investigating the La Niña–like trend further.

One might wonder how to reconcile the strengthening Walker circulation in the M model with the robust conclusion from the energy and water balances that the atmospheric circulation should weaken under global warming (Held and Soden 2006). It is important, however, to remember that this explanation only constrains

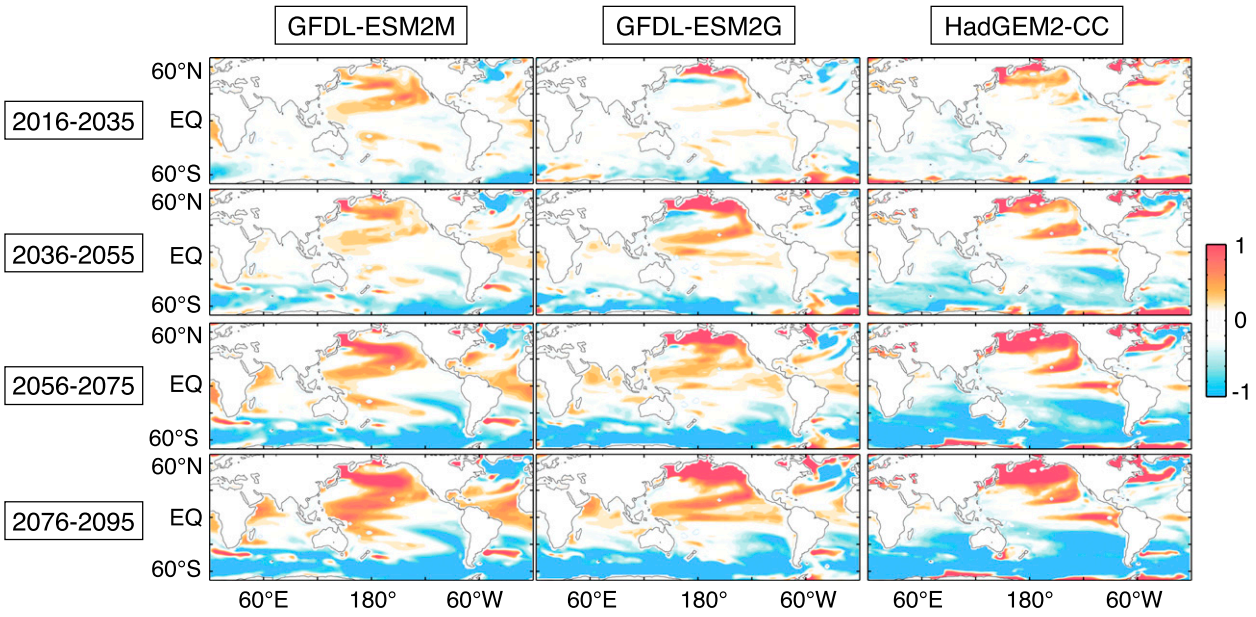

FIG. 2. (left) Bidecadal mean SST (deviations from the global mean) in GFDL-ESM2M under RCP 8.5, starting from 2016, 2036, 2056, and 2076, computed relative to the decadal mean SST starting from 2006. Unit is °C (100 yr)$^{-1}$. (middle) As at left, but for GFDL-ESM2G. (right) As at left, but for HadGEM2-CC.

the global mean change. The scatterplots in Fig. 4a show the relationship between the annual-mean temperature change and the precipitation increase under RCP 8.5 expressed with respect to the mean over 2006–15. Also shown are the least squares best fit line of the precipitation increase and the estimated increase of water vapor due to the Clausius–Clapeyron relationship (7% K^{-1}) assuming that the relative humidity remains constant. The explanation given by Held and Soden (2006) is that, to increase precipitation more slowly than 7% K^{-1}, the water vapor increase has to be compensated by weakening atmospheric circulation. In the majority of global climate models including the M and Had models, this is true for the global-mean circulation as shown in Fig. 4a. Figure 4b clearly shows that the vertical motion at 500 hPa in the M model is weakening globally except for the tropical Pacific and a few other places. Therefore, the strengthening Walker circulation in the M model does not violate the conclusion derived from the global energy and water balances.

4. Fundamental constraint between the multidecadal SST variability and the ENSO amplitude changes imposed by realistic ENSO nonlinearity, and their warming responses

In this section, we first focus on multidecadal natural variability of the tropical SST to show that, if the nonlinearity of ENSO is realistic, multidecadal variations of the zonal SST gradient are fundamentally tied to the ENSO amplitude variations. The M model reproduces this observed constraint remarkably well, but the G and Had models violate this constraint because these two models do not reproduce the observed ENSO nonlinearity. We then demonstrate that the La Niña–like trend in the M model is a forced response to global warming, which appears to be causally related to the weakening ENSO amplitude.

a. The role of ENSO nonlinearity in multidecadal SST natural variability

Before exploring the warming response further, we take a step back and investigate the relationship between the zonal SST gradient and the ENSO amplitude in natural variability. Specifically, we first analyze an observational dataset and the piControl runs of the models. The upper panels of Figs. 5a and 5b show the 11-month running mean SST averaged over the Niño-3 region (5°S–5°N, 150°–90°W; shown as a black box in the lower panel) for two successive 95-yr time spans starting from year 211 and year 306 in the piControl run of the M model. The earlier (later) time span is chosen to show an example of the era when the ENSO amplitude exhibits a substantial decrease (increase). Interestingly, the lower panels of Figs. 5a and 5b show a well-defined La Niña–like trend (years 211–305) and an El Niño–like trend (years 306–400), respectively.

Except during large El Niño events, the Niño-3 SST shown in Fig. 5 remains about 24°C. Therefore, at least

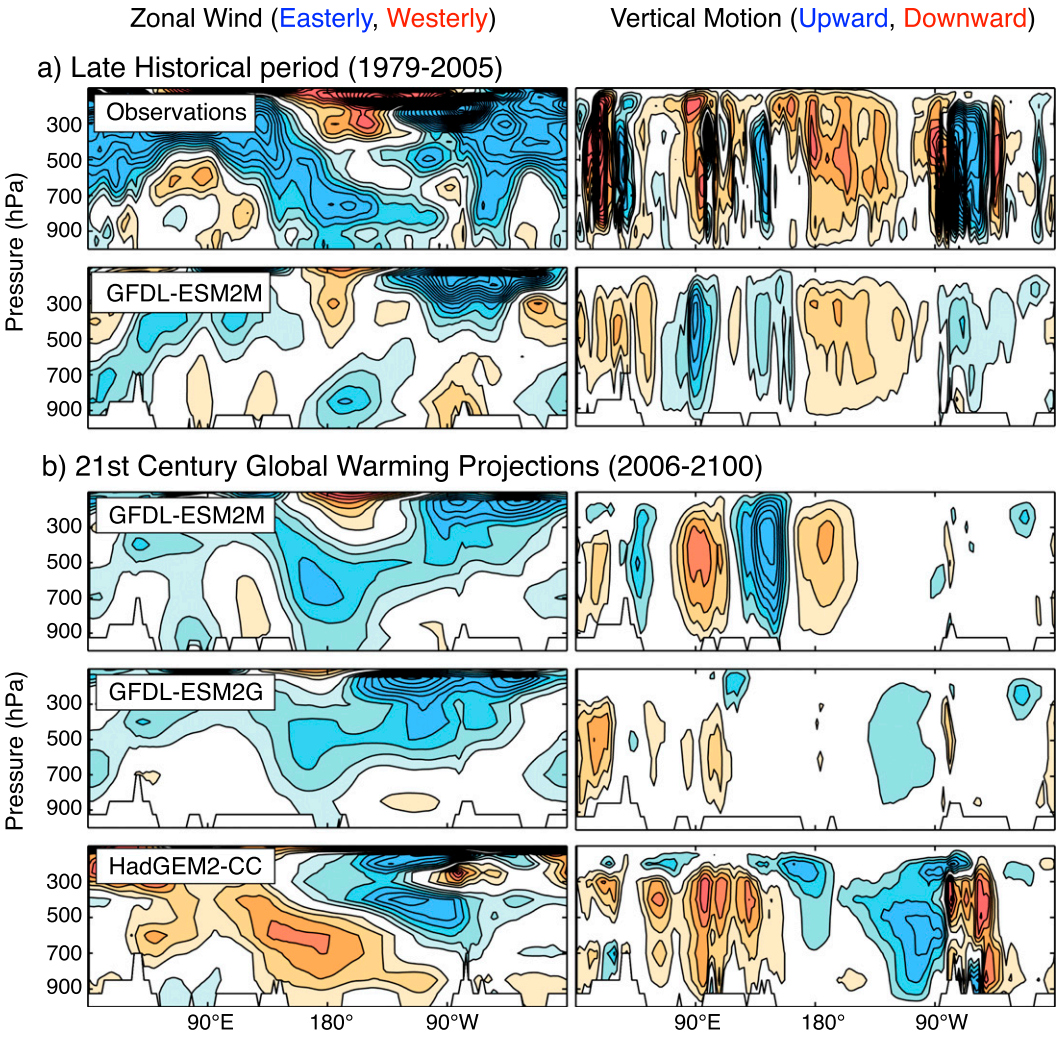

FIG. 3. (a) Observed and simulated equatorial (10°S–10°N) meridional mean trends of (left) zonal wind and (right) vertical motion during the late historical period. Observations are from the ERA-Interim dataset, and the model output is from the historical runs of GFDL-ESM2M. Contour interval is 0.2 $(\mathrm{m\,s^{-1}})(27\,\mathrm{yr})^{-1}$. Zero contours are omitted, and easterly (westerly) anomalies are shaded blue (orange). Contour interval is 2 $(\mathrm{hPa\,day^{-1}})(27\,\mathrm{yr})^{-1}$. Upward (downward) anomalies are shaded blue (orange). (b) As in (a), but for GFDL-ESM2M, GFDL-ESM2G, and HadGEM2-CC under RCP 8.5. Contour intervals are 0.5 $(\mathrm{m\,s^{-1}})(100\,\mathrm{yr})^{-1}$ for zonal wind and 3 $(\mathrm{hPa\,day^{-1}})(100\,\mathrm{yr})^{-1}$ for vertical motion.

in the M model, it is more reasonable to assume that the centennial SST trends in piControl are just a manifestation of the ENSO amplitude modulations rather than that the mean state is modulated by some other factors, such as heat advection from the extratropical regions. It is easy enough to understand why the ENSO amplitude variations can rectify the multidecadal SST trends (e.g., Battisti and Hirst 1989; Jin et al. 2003; An et al. 2005; Atwood et al. 2017). For example, the upper panels of Fig. 5 show that the SST probability distribution in the M model is highly skewed toward stronger, less frequent El Niños and weaker, more frequent La Niñas. Therefore, if ENSO becomes inactive and the number of large El Niño events decreases, then the mean state is rectified to be La Niña–like, and vice versa. An important implication from Fig. 5 is that, to provide a realistic global warming projection of the mean-state SST trends, it is essential for models to reproduce both the ENSO nonlinearity and the ENSO amplitude trends, in addition to mean-state changes that are independent of the ENSO response to warming.

In the real world, it is also widely known that ENSO is not a linear phenomenon. The aforementioned asymmetry of ENSO is clearly observed during the satellite era. The lower panel of Fig. 6 shows that large El Niño events with SST anomalies of 2°C or more happened in

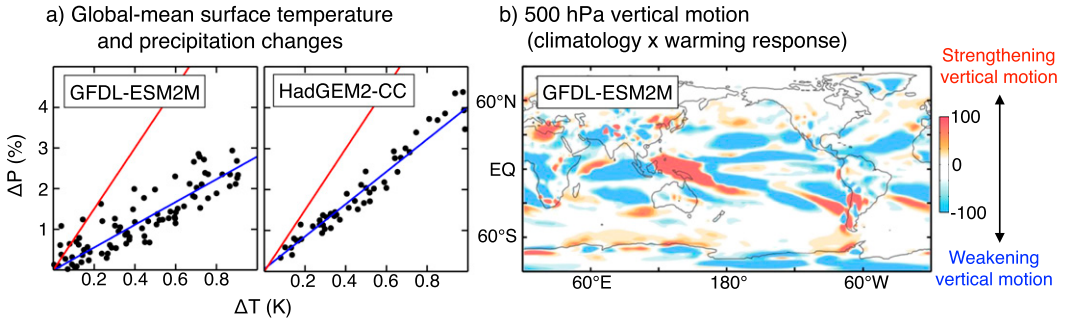

FIG. 4. (a) Scatterplots showing the relationship between the global mean surface temperature change and the global precipitation change in two models under RCP 8.5. Each dot represents annual mean computed relative to the mean over 2006–15. The least squares best fit lines are shown in blue, and the estimated increase of water vapor due to the Clausius–Clapeyron relationship (7% K^{-1}) in red. (b) Product of climatology and warming response in 500-hPa vertical motion of GFDL-ESM2M under RCP 8.5. Climatology is the means over 2006–35, and the warming response is the epochal differences between 2070–99 minus 2006–35. Unit is (hPa day^{-1})^2.

1982/83 and 1997/98 in this metric. On the other hand, the La Niña anomalies are always about 1°C but are realized more frequently. For an objective measure, skewness of the detrended Niño-3 SST anomalies is 0.61 for the entire time span shown in Fig. 6 (positive skewness means stronger, less frequent El Niños and weaker, more frequent La Niñas). The mechanism to yield this ENSO asymmetry is comprehensively discussed by Battisti and Hirst (1989) and An and Jin (2004).

This nonlinearity motivates us to define two SST indices between which we expect a reasonably high correlation. The blue curve in the upper left panel of Fig. 6 shows the 7-yr running standard deviation (RSTD) of Niño-3 SST. This index represents whether the ENSO is active or inactive in the given 7-yr window. The red curve shows the zonal SST gradient (ZSG) index defined as the 7-yr running mean of the SST difference calculated in the manner of Niño-3 minus Niño-4 (5°S–5°N, 160°E–150°W; shown as a black box in the lower panel of Fig. 5a). By definition, a positive (negative) ZSG index represents an El Niño–like (La Niña–like) mean state in the given 7-yr window. Both the RSTD and ZSG indices are expressed in unit of °C and the means over the entire record are removed beforehand. Because the typical ENSO period is about 3–5 years, we use the window length of 7 years so that the window covers at least one full cycle. Nevertheless, even if 11-yr windows are used, similar results are obtained (not shown). This insensitivity confirms that our results are reasonably window-length independent, so

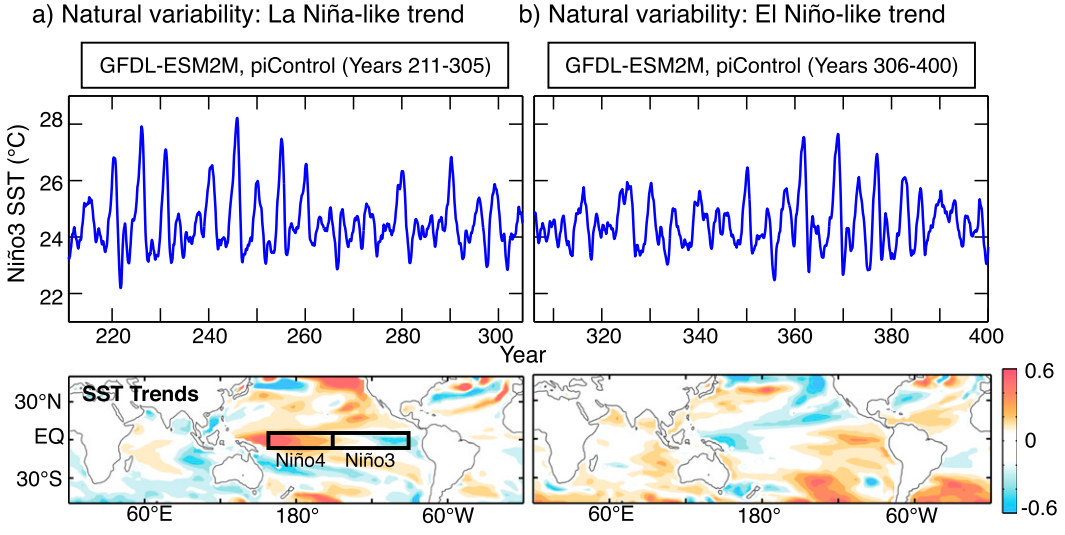

FIG. 5. (top) SST averaged over the Niño-3 region (5°S–5°N, 150°–90°W) simulated by GFDL-ESM2M under the preindustrial control (piControl) run. Monthly climatology is not subtracted, but 11-month running mean is applied. (bottom) As in Fig. 1c (bottom), but for piControl. The Niño-3 and -4 regions are shown by the black boxes. Years (a) 211–305 and (b) 306–400 are shown.

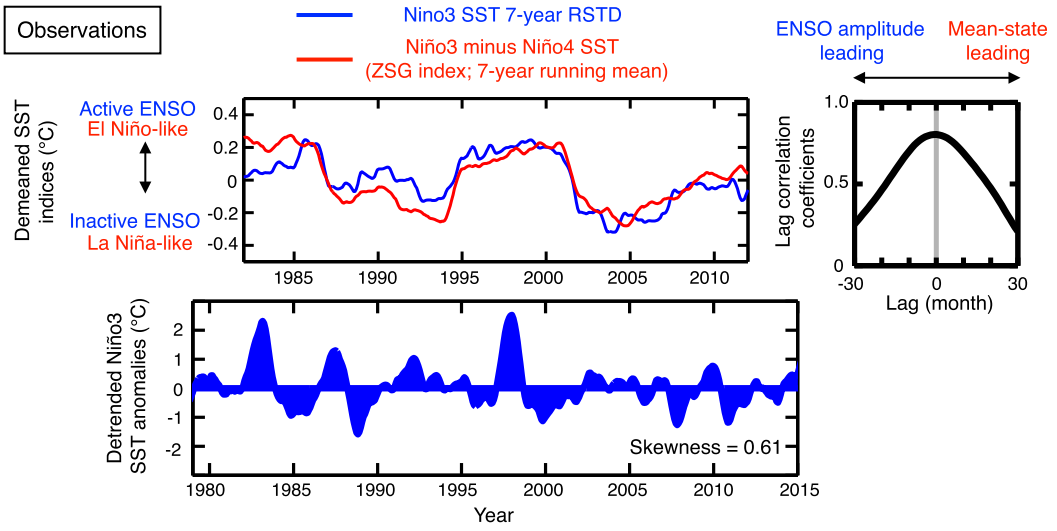

FIG. 6. (top left) Blue indicates observed 7-yr running standard deviations (RSTD) of the Niño-3 SST. RSTD is calculated to represent deviations from the running mean state at each window. Means over the entire time span are removed. Red indicates observed zonal SST gradient (ZSG) index defined as the difference "Niño-3 minus Niño-4" SST for the three runs. A 7-yr running mean is applied. Means over the entire time span are removed. (top right) Lag correlation coefficients between the two indices calculated over the time series. Positive (negative) lags mean the Niño-3 RSTD is lagging (leading) the ZSG index. (bottom) Observed detrended Niño-3 SST anomalies. 11-month running mean is applied. Skewness calculated over the entire period is shown at the bottom right.

we hereafter use the 7-yr window to yield more statistical degrees of freedom.

A trivial reason why the two indices should be highly correlated is as follows. If a 7-yr window contains a large El Niño event, the ENSO is defined as "active" and the zonal SST gradient tends to be more El Niño–like in the 7-yr time span, suggesting that both indices are likely to be positive. On the other hand, if a 7-yr window does not contain a large El Niño event, the ENSO is generally "inactive" and the zonal SST gradient is relatively La Niña–like, suggesting that both indices tend to be negative. Here, the important effect of the ENSO nonlinearity is that, even if the window contains a large La Niña event, the RSTD does not become as large as El Niño counterparts. Whenever ENSO is more active than the norm, more El Niño–like phases are expected rather than La Niña–like phases.

As expected, the two indices exhibit a remarkably high correlation of >0.8 without any detectable lags during the satellite era (Fig. 6, top panels). In particular, both indices are higher than the norm in the years whose 7-yr window includes the large El Niño event in 1997/98. It is also evident that the phase of low-frequency variability is determined by the occurrence of El Niño events rather than La Niña events. This asymmetry appears to be because the amplitude of El Niño events tends to vary substantially, but that of La Niña events remains almost constant throughout the entire time span. This observed evidence implies that the ENSO nonlinearity plays an important role in low-frequency SST variations in the equatorial Pacific. We have also detected statistically significant correlations between the two indices using longer records (e.g., correlation = 0.54 for 1921–2015 in HadISST; significant at the 95% confidence level), but the uncertainty due to sparse observations is so large that the two indices before the satellite era is highly dataset dependent.

b. *Preindustrial control runs with and without realistic ENSO nonlinearity*

Next, to further confirm the importance of the ENSO nonlinearity, we use the three models introduced in the former sections. Figure 7 shows that the M model exhibits strong nonlinearity (skewness = 0.98), whereas the G (skewness = 0.09) and Had (skewness = −0.05) models exhibit weaker nonlinearity. Because the G model is different from the M model only by its oceanic component, this difference in nonlinearity must originate from the oceanic configurations. The Had model exhibits a negative skewness, suggesting that La Niña events tend to be larger than El Niño events at least in this particular run. Preliminary analyses suggest that many other CMIP5 models also fall into this unrealistic "negative skewness" category (not shown), but we will focus on the Had model in this study.

If the ENSO nonlinearity is not realistically simulated, the nonlinear rectification effect on the mean-state zonal SST gradient should also be unrealistic. In other words, we have an a priori reason to expect that the correlations between the RSTD and ZSG indices should be lower in

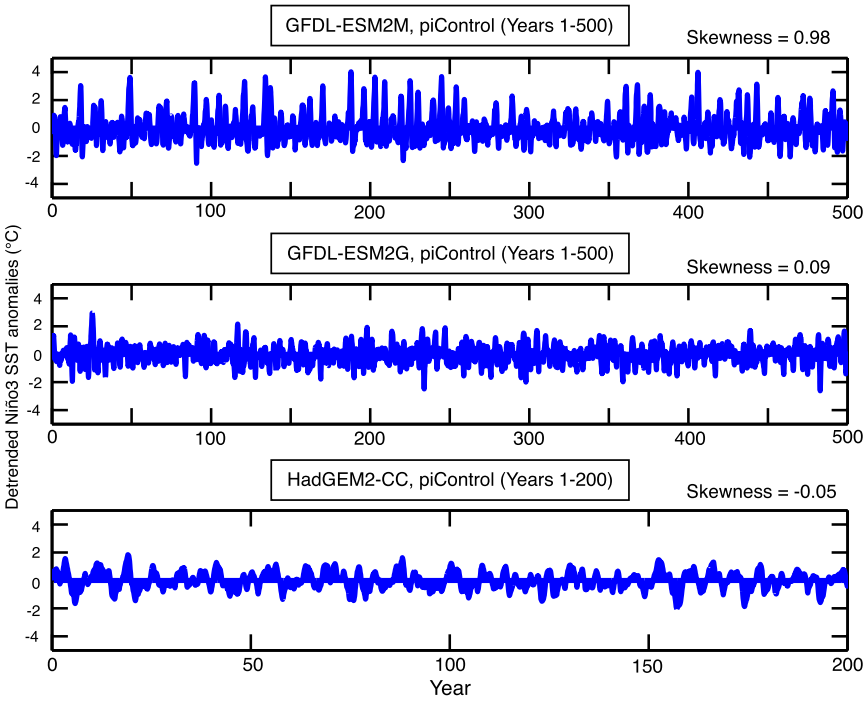

FIG. 7. As in the bottom panel in Fig. 6, but for the piControl runs of the three models. Note that the length of the time span for HadGEM2-CC is different from the two GFDL models. Skewness calculated over the entire period are shown at the top right.

the G and Had models than in the M model. The two indices of the three models calculated from the piControl runs verify this expectation (Fig. 8). The time series simulated by the M model over five centuries clearly shows that the ENSO amplitude and the mean-state zonal SST gradient are tightly interconnected (correlation = 0.8–0.9), whereas those in the G model only exhibit a moderate correlation (correlation = 0.4–0.5). The correlation in the Had model is even lower (correlation = 0.1–0.2), and during some time spans (e.g., years 150–180) the two indices are anticorrelated. This may be a manifestation of negative skewness, which is particularly evident in those periods (Fig. 7, bottom).

The lag correlation property of the M model suggests that the ENSO amplitude leads the mean-state zonal SST gradient by about 10 months. Even if we divide the 500-yr time series into centuries and calculate the correlations separately, this lag correlation robustly appears in all five centuries (not shown). This slight lead–lag relationship is consistent with the idea that the ENSO variations cause the mean-state SST modulation within a nonzero time lag, but based on the short record of observations, it is hard to determine whether this modeled lag is realistic. Nevertheless, the evidence that the mean state is lagging, rather than leading, support the notion that the ENSO amplitude does not simply respond to mean-state changes caused by other factors. This notion is consistent with a recent finding by Atwood et al. (2017), who showed using a different GFDL model, GFDL CM2.1, that the mean-state natural variability is an effect, rather than a cause, of the ENSO amplitude variability. The causality between the mean state and the ENSO amplitude will be further discussed in the next section.

c. *Forced ENSO weakening and the La Niña–like response to global warming in the M model*

In the former subsections, we have shown that large centennial variations of the zonal SST gradient could result from natural variability of ENSO amplitude variations. Although some strong La Niña–like trends are realized in the piControl run, this large natural variability does not necessarily mean that the La Niña–like trend under warming experiments in the M model should be also regarded as pure natural variability.

The upper panels of Fig. 9 show the strength of anthropogenic forcing for the historical (years 1860–2005), RCP 8.5 (years 2006–2100), and Abrupt4xCO2 runs (years 101–300 only). For Abrupt4xCO2, only data after year 100 are shown because it takes several decades before the system reaches its quasi-equilibrium. For the former two experiments, the forcing exhibits a monotonic increase; in particular, the forcing experiences a more rapid increase after the beginning of the satellite era. Then, the forcing becomes stronger following the RCP

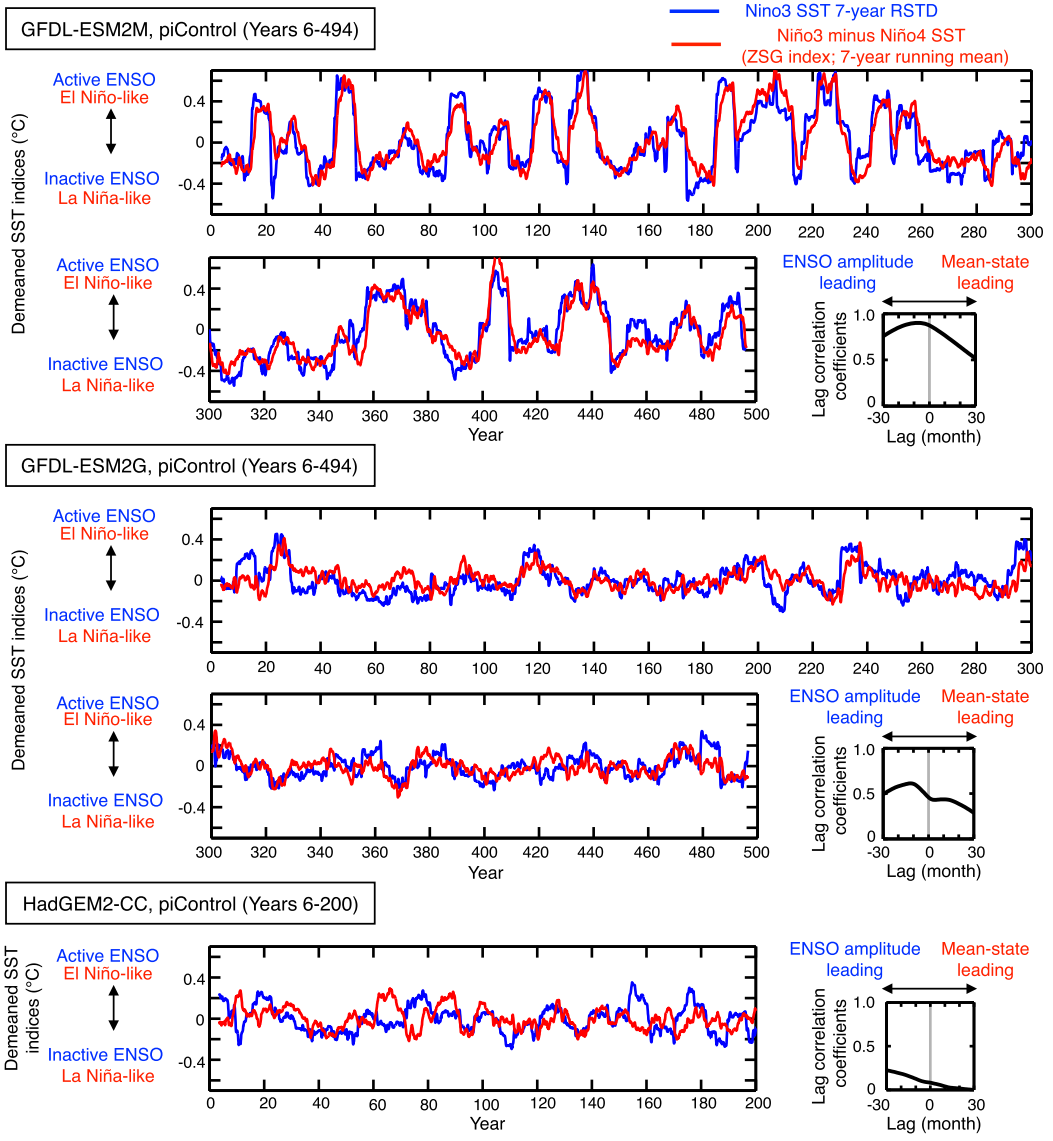

FIG. 8. As in the top panels in Fig. 6, but for the piControl runs of the three models. Note that the length of the time span for HadGEM2-CC is different from the two GFDL models.

8.5 scenario to reach a level comparable to the quadrupling of CO_2 at the end of this century.

The lower panels of Fig. 9 show the same indices as in the piControl runs but for the runs under the anthropogenic forcing described in the last paragraph. Here the indices are expressed relative to the means over piControl. During most of the historical period, natural variability of both indices is as large as in the piControl run. After the beginning of the satellite era, however, the two indices gradually start to decrease to reach the level of the quadrupled-CO_2 run, in which ENSO amplitude and its decadal variations are substantially weakened. In accordance with this weakened amplitude, the mean-state zonal SST gradient in the warmer climate remains La Niña–like at least for at least two centuries. By comparing the piControl run (Fig. 8, top) and the Abrupt4xCO2 run (Fig. 9, bottom right) in the M model, it is virtually certain that the weakening ENSO and the La Niña–like shift in the M model are forced responses to global warming, rather than a manifestation of natural variability. The historical and RCP 8.5 runs smoothly connect the two regimes, exhibiting a clear transition toward a warmer climate.

Furthermore, to statistically verify that the ENSO weakening is a forced response, we have calculated the 3-yr RSTD of the Niño-3 SST in the M model, and this

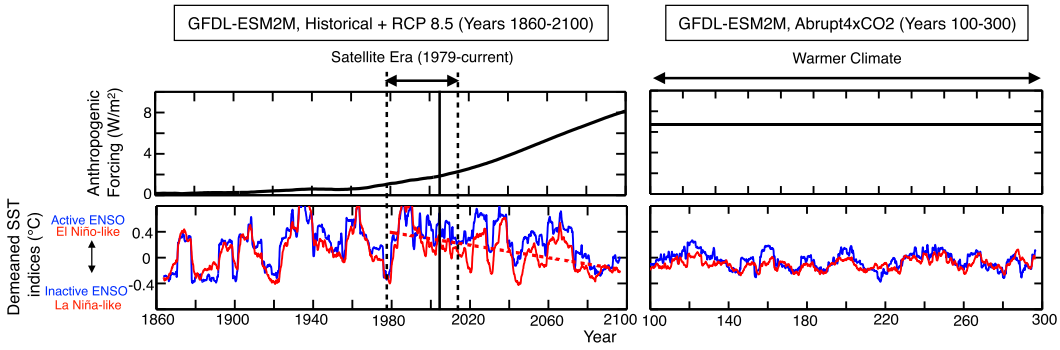

FIG. 9. (top) Strength of anthropogenic forcing for the historical, RCP 8.5, and abrupt quadrupling carbon dioxide (Abrupt4xCO2) runs. For Abrupt4xCO2, only after Year100 is shown because it takes several decades before the system reaches its quasi-equilibrium. The equilibrated value of the anthropogenic forcing in the Abrupt4xCO2 run (6.72 W m^{-2}) is estimated by Andrews et al. (2012). (bottom) As in the top panel of Fig. 8, but for the experiments shown in the top panels. The indices are expressed relative to the means over the entire time span of piControl shown in Fig. 8. The dashed line shows the least squares best fit line calculated from 1979–2100.

time series exhibits a significant decrease of the ENSO amplitude at the 95% confidence level (not shown). To show that this amplitude decrease is unlikely to be a result of natural variability, we have then performed the same analysis using the first 2000 years of the 4000-yr-long preindustrial control run of GFDL CM2.1. Specifically, we have calculated the significance of the amplitude trends for every possible time span with length of 95 years (i.e., years 2–96, 3–97, . . . , and 1904–99, starting from year 2 because we calculate 3-yr RSTD). Surprisingly, out of the two millennia, only eight time spans that can be sorted into three eras—era 1 (95-yr time spans starting from years 125, 126, 127, and 128), era 2 (starting from years 297, 298, and 299), and era 3 (starting from year 1716)—have experienced significant amplitude decrease at the 95% confidence level. In addition, none of them has shown a steeper trend than the RCP 8.5 run of the M model. Although the source of the ENSO nonlinearity in GFDL CM2.1 appears to be different from that of the M model (Atwood et al. 2017), GFDL CM2.1 is similar to the M model in many respects (Dunne et al. 2012) including the nonlinear rectification effect and the strengthening Walker circulation in response to warming (Tanaka et al. 2005). These statistical analyses also strongly suggest that the ENSO response in the M model is forced.

An important conclusion derived from this subsection is that, to the best of our knowledge, it is very likely that the significant ENSO weakening and the La Niña–like mean-state response in the M model are a forced response to global warming, rather than centennial natural variability. In addition, by analyzing the historical run of the M model, the case has been made that the forced response could have been detectable since the late twentieth century. Then, our next question would be whether the real world behaves like the M model or the other models, but this question is much harder (perhaps impossible) to address. Nevertheless, our analysis suggest that the forced La Niña–like response in the M model appears to be tied to the nonlinearity of ENSO, and that the nonlinearity in the M model is more realistic than those in some other CMIP5 models. In particular, the contrast between the M and G models undoubtedly sheds new light on the role of upper oceanic properties, particularly the ENSO nonlinearity, in determining the mean-state SST response to global warming.

As long as a model simulates realistic ENSO nonlinearity and weakening ENSO amplitude, the aforementioned La Niña–like forcing mechanism at least competes with the other mechanisms that favor El Niño–like warming. Based on the large ENSO amplitude and the strong ENSO nonlinearity of the M model, we could argue that the M model is an exception among the state-of-the-art GCMs due to the strong nonlinear rectification effect. Although the evidence discussed in this study is not enough to conclude that the M model simulates the zonal SST gradient response more realistically, it lends confidence to the notion that the La Niña–like warming scenario may be as reasonable as the El Niño–like warming scenario, since consistent physical mechanisms can be outlined. Considering the fact that previous studies have not reached consensus on how the ENSO amplitude will change under global warming (e.g., Collins et al. 2010), a La Niña–like mean-state response to warming remains a plausible outcome.

5. Discussion on hypothetical physical mechanisms to yield the intermodel differences

In the previous section, we have mainly discussed the role of the ENSO nonlinearity and the amplitude response in constraining the mean-state response to global

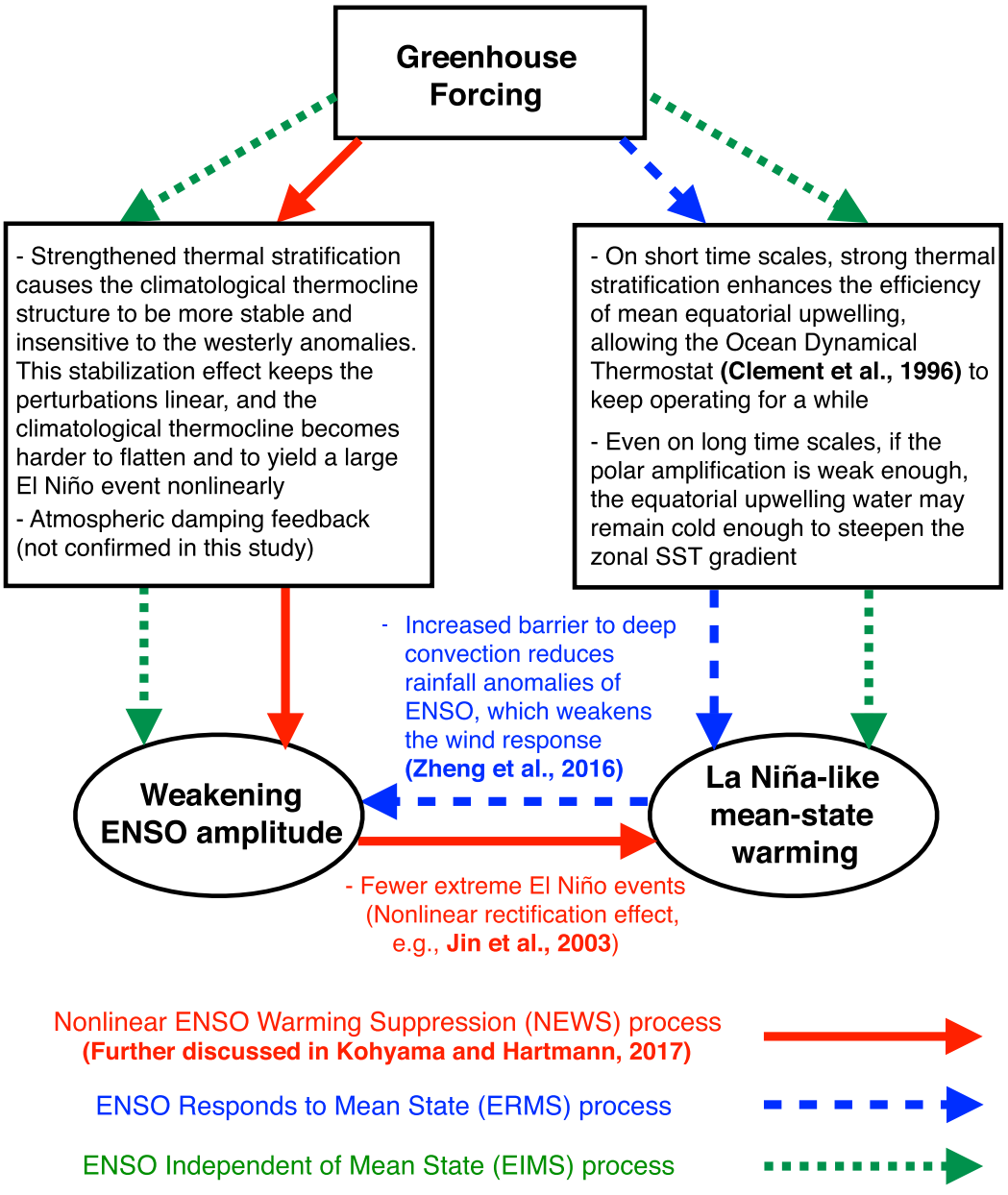

FIG. 10. Three possible causal processes among greenhouse forcing, the ENSO amplitude change, and the La Niña–like mean-state response in GFDL-ESM2M. Also shown are examples of physical mechanisms that are potentially important.

warming. The "nonlinear rectification effect" of natural ENSO variability on the mean state was comprehensively discussed by Battisti and Hirst (1989), Jin et al. (2003), and An et al. (2005), for instance. Atwood et al. (2017) recently showed using GFDL CM2.1 that the mean-state SST decadal variability appears to be just a manifestation of the ENSO amplitude variability. Therefore, as in the M model, if a model simulates realistic ENSO nonlinearity, and if ENSO is forced to weaken by global warming, then the nonlinear rectification effect causes a suppression of mean-state warming in the eastern equatorial Pacific, yielding a La Niña–like trend. We refer to this process as "nonlinear ENSO warming suppression" (NEWS; see Fig. 10, red solid arrows) and have discussed it further in Kohyama and Hartmann (2017).

On the other hand, many other studies suggest that the mean-state response is the cause, rather than the effect, of the ENSO amplitude changes. For example, by sorting the CMIP5 models into El Niño–like and La Niña–like categories, Zheng et al. (2016) concluded that, "in models

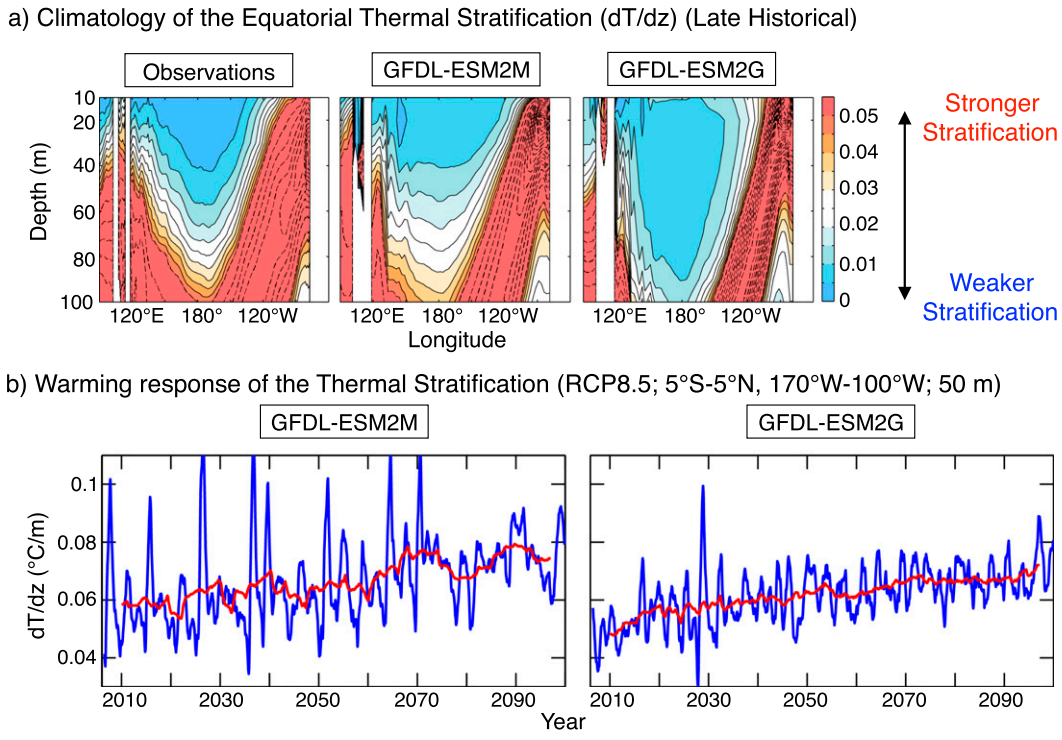

FIG. 11. (a) Climatological meridional-mean thermal stratification (dT/dz) over 5°S–5°N in late historical period (1980–2005) for observations and the two GFDL models. Unit is °C m^{-1}. Contour intervals are 0.005°C m^{-1} below 0.05°C m^{-1} (solid curves), and 0.02°C m^{-1} above 0.05°C m^{-1} (dashed curves). (b) Regional mean thermal stratification averaged over 5°S–5°N, 170°–100°W at the 50-m depth under the RCP 8.5 scenario. The 3-yr (8 yr) running mean is applied for the blue (red) curve.

with an enhanced mean warming in the eastern equatorial Pacific, the barrier to deep convection is reduced, and the intensified rainfall anomalies of ENSO amplify the wind response and hence SST variability'' (p. 7265) and vice versa. Some other mechanisms are also discussed in Collins et al. (2010). Therefore, if a certain mechanism favors the La Niña–like mean state, this mechanism can cause the weakening ENSO amplitude. To contrast this mechanism with NEWS, we refer to this process as ''ENSO responds to mean state'' (ERMS) (Fig. 10, blue dashed arrows). In addition to NEWS and ERMS, we could also outline a third possibility in which the La Niña–like mean state warming and the weakening ENSO amplitude are independently forced by global warming. We refer to this third process as ''ENSO independent of mean state'' (EIMS) (Fig. 10, green dotted arrows). We believe, however, EIMS is less likely to be a dominant process, considering the remarkably high correlation between the RSTD and ZSG indices.

The three possible causal processes (i.e., NEWS, ERMS, and EIMS) and some examples of physical mechanisms are summarized in Fig. 10 as a potential mechanism to explain the La Niña–like trend in the M model. These mechanisms involve the direction of causality between the zonal SST gradient, ENSO amplitude, and greenhouse gas warming. Although it is not clear which process in Fig. 10 is the most important one, we have good evidence to assume that some important oceanic mechanisms must control the zonal SST gradient response to warming, because the M and G models are different only in their oceanic components. In this section, we list some potentially important mechanisms for simulating the La Niña–like warming pattern in the M model by comparing it to the G model.

a. Potential roles of the climatological thermal stratification and its warming response

One of the major climatological differences in the equatorial Pacific between the M and G models is thermal stratification. Here, thermal stratification is defined as the temperature difference between adjacent depth levels (dT) divided by the vertical distance between them (dz). Figure 11a shows the climatological thermal stratification over the equatorial Pacific for observations and the two GFDL models during the late historical period. The upper ocean stratification of the M model (and the real world) is generally stronger in the 40–100-m layer in the equatorial Pacific than that of the

G model, which means that the mean and variance of vertical heat advection across the subsurface tend to be larger in the M model. In particular, this larger variance of advection is generally associated with the larger ENSO amplitude, which might also indirectly influence the magnitude of the nonlinear rectification effect on the mean-state trends (see Figs. 7 and 8).

In addition, Fig. 11a implies that the mixed layers in the M model and the real world are shallower than that in the G model. If the mixed layer is shallower, the surface heat flux and the Sverdrup transport can more easily recharge the heat into the mixed layer and collapse the climatological thermocline drastically enough for the anomalies to deviate from the range of ''linear'' perturbations. This deviation from the linear regime is essential to yield the ENSO asymmetry and large El Niño events (An and Jin 2004). Therefore, the difference in mixed layer depth is consistent with the evidence that the ENSO nonlinearity is more realistically simulated by the M model than the G model.

The explanations in the previous paragraphs support the NEWS process as a possible cause to simulate the La Niña–like response. On the other hand, the evidence that the M model is more stratified means that the mean equatorial upwelling cools the surface more efficiently. At least in a shorter time scale than a couple of decades, the efficient climatological upwelling would favor the La Niña–like mean-state response due to the ocean dynamical thermostat (Clement et al. 1996). Although it is not clear whether this mechanism continues to operate in a longer time scale, the difference in the equatorial thermal stratification is at least consistent with the ERMS process as well.

In Fig. 11b, we also show the warming response of the regionally averaged (5°S–5°N, 170°–100°W) equatorial thermal stratification at the 50-m depth (i.e., the typical observed mixed layer depth on the equatorial Pacific). As the climate warms, the climatological stratification consistently strengthens in both models, so one might suspect that no important difference is evident in the warming response. The stronger climatological thermal stratification of the M model, however, also has an implication for this warming response. If the equatorial upwelling becomes more efficient than a certain threshold value, the thermocline will be so stabilized that it becomes less likely for the climatological thermocline to collapse. The system, then, no longer yields a large El Niño event, causes the ENSO nonlinearity to dissipate, and weakens the ENSO amplitude. In Kohyama and Hartmann (2017), we have shown that this mechanism can be simulated by an idealized model with nonlinear ENSO. Assuming that this mechanism is realistic, we could speculate based on the left panel of Fig. 11b that the thermal stratification in the M model appears to ''saturate'' after about 2070 under RCP 8.5, which causes large El Niño events to die out. Hence, the warming response could also be essential for the intermodel difference in the capability of simulating the NEWS process, and therefore, the La Niña–like mean-state response.

We could speculate that the ultimate cause of the aforementioned difference in upper ocean properties might be related to the difference of equatorial vertical diffusivities. The equatorial diffusivities in the G model below the surface boundary layer are generally small, partly because the interior background values in the G model are parameterized near the equator based on a presumed f dependence for near-inertial wave–wave interactions (Harrison and Hallberg 2008). As the first step, the influence of vertical diffusivity on the mean-state warming response could be tested by analyzing model runs with different background diffusivity values. Nevertheless, the difference of total diffusivity also depends upon the shear mixing scheme, the boundary layer model, the vertical resolution, and the mixing due to truncation errors, so further comprehensive analyses and model runs are needed to determine the root cause of the overall intermodel difference.

b. *Potential mechanism related to the strength of polar amplification*

From a more global perspective, we could argue that the strength of polar amplification of global warming may support the ERMS process. Figure 12a shows the difference map of the trends of SST (deviations from the global mean) between the M and G models. This map shows that the polar amplification of global warming is weaker in the M model, especially in the eastern Pacific basin. We obtain a similar result between the M and Had models as well (not shown). Therefore, we could hypothesize that the advection of this cooler water might contribute to the cooler equatorial upwelling, because the outcrops of climatological isopycnal surfaces from which the upwelling water originates are generally observed at higher latitudes (Fig. 12b).

Figure 12c shows the difference of the temperature warming response between the two models, juxtaposed with the climatological isopycnal surfaces in the M model. The temperature anomalies reasonably match the climatological isopycnal surfaces, which suggests that the potential temperature anomalies are following the Lagrangian transport of seawater. In particular, the cold anomalies of the northeast Pacific clearly extend to the eastern equatorial Pacific later this century. With the help of the ocean dynamical thermostat mechanism, this extratropical oceanic teleconnection can cause the La

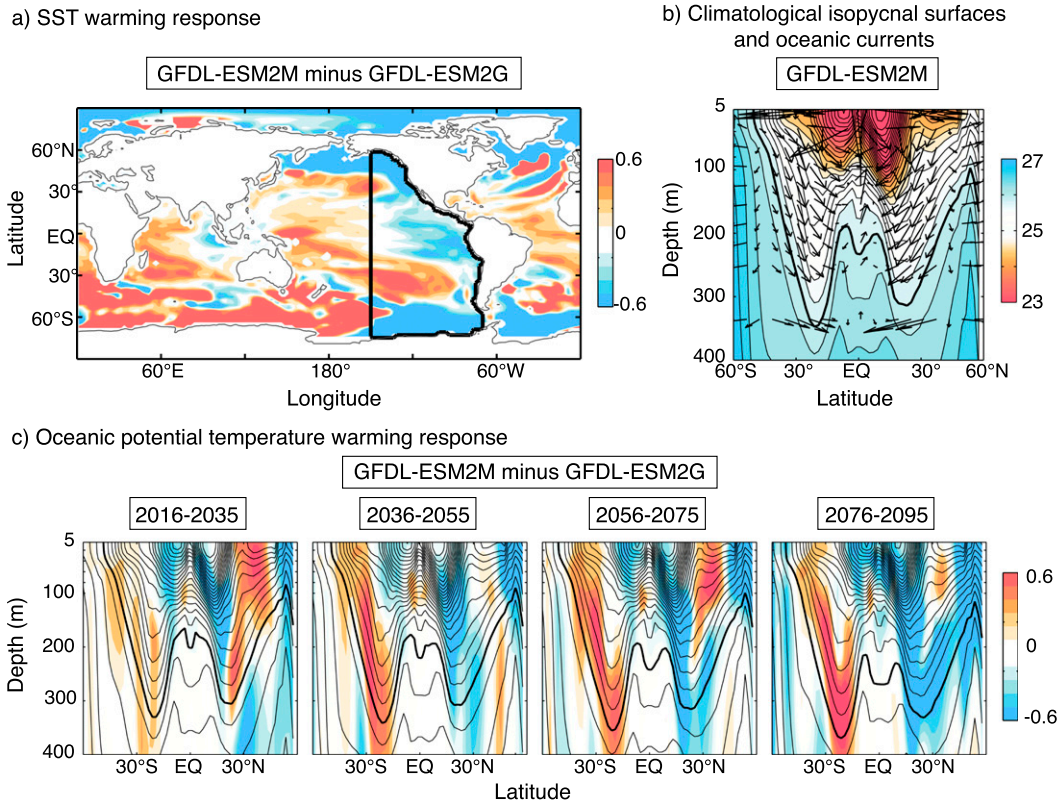

FIG. 12. (a) Difference of the SST (deviations from the global mean) trends between the two GFDL models under RCP 8.5. Unit is °C $(100\,\mathrm{yr})^{-1}$. The region surrounded by the black curve is the area for which the zonal means shown in (b) and (c) are calculated. (b) Contours indicate climatological zonal-mean potential density under RCP 8.5 (2006–2100) for GFDL-ESM2M over the eastern Pacific region shown in (a). Unit is $\mathrm{kg\,m^{-3}}$, but $1000\,\mathrm{kg\,m^{-3}}$ is subtracted following the conventional notation. Contour interval is $0.2\,\mathrm{kg\,m^{-3}}$, and the bold contour shows the $26\,\mathrm{kg\,m^{-3}}$ isopycnal surface. Arrows indicate the same as contours, but the meridional and vertical mass transport are qualitatively shown. The vertical component is stretched by a factor of 5 for the purpose of visualization. (c) Contours are as in (b), but for bidecadal mean potential density starting from 2016, 2036, 2056, and 2076. Shadings show the warming response of potential temperature computed relative to GFDL-ESM2G. The warming response is computed as the bidecadal means relative to the decadal mean potential temperature starting from 2006. Unit is °C. Note that the contours show the climatology of GFDL-ESM2M, while the shadings show the intermodel difference of the warming response.

Niña–like trend in this model and, in turn, the weakening ENSO based on the ERMS process. Actually, despite the problem of the ocean dynamical thermostat mentioned in the introduction section, Seager and Murtugudde (1997) validated the dynamical damping mechanism in eastern equatorial Pacific in an oceanic GCM experiment even in the presence of midlatitude ocean warming. One possibility to explain their result might be that, if the polar amplification is weak enough, then the ocean dynamical thermostat might remain valid for a longer time scale than the majority of the CMIP5 models suggest.

Nevertheless, a caveat of this mechanism is that some earlier studies suggest that a large portion of the water in the undercurrent comes from the Southern Hemisphere subtropics (Tsuchiya et al. 1989; Rodgers et al. 2003; Goodman et al. 2005). The anomalies could also be associated with the intermodel difference of heaving, rather than mass transport. Further investigations and some model experiments are needed to verify this hypothesis.

6. Summary and concluding remarks

We have shown that GFDL-ESM2M (the M model) is an interesting outlier in the CMIP5 models, because it exhibits a La Niña–like response to global warming in the equatorial Pacific. GFDL-ESM2G (the G model), which differs from the M model only in the oceanic components, does not yield well-defined La Niña–like warming. Using this difference, we have explored the potential oceanic roles that may be important for the difference in the trends of the zonal SST gradient in

the equatorial Pacific. We have also compared the M model with HadGEM2-CC (the Had model), which exhibits a typical El Niño–like trend that resembles the multimodel mean response to warming.

First of all, in section 3, we have clarified that the La Niña–like warming in the M model is a gradual process that takes almost a full century to reach the mature phase. Then, we have shown that the Walker circulation change associated with the La Niña–like response in the M model has the same sign as the observed change during the late historical period, and the spatial structure of the circulation becomes more similar under RCP 8.5 to what we have observed thus far, which is opposite to the Had model (and the multimodel mean) project. We are interested in investigating whether the recent strengthening Walker circulation could be partly forced by global warming, but the short record of the late historical period by itself cannot be used to answer this question. Therefore, in the following section, we have further investigated the piControl and Abrupt4xCO2 runs, as well as the historical and RCP 8.5 runs, to show that the La Niña–like response in the M model is, actually, very likely to be forced.

In section 4, we have first shown that, given the realistic ENSO nonlinearity, the centennial natural variability must be fundamentally constrained by the ENSO amplitude variability. In both observations and the M model, the probability distribution of ENSO is generally skewed toward stronger, less frequent El Niños and weaker, more frequent La Niñas. Therefore, a time span with active ENSO should trivially correspond to a time span with an El Niño–like mean state, and vice versa, as long as the ENSO nonlinearity is realistically simulated. The G and Had models violate this relationship, however, because the ENSO nonlinearity in these models are not realistic. An important conclusion from this section is that, to project a mean-state SST trend realistically, it is necessary for models to reproduce the following three properties: the ENSO nonlinearity, the ENSO amplitude variability, and the mean-state changes that are independent from the ENSO response to warming.

At least in the M model, by comparing the piControl and Abrupt4xCO2 runs, we can argue with very high confidence that the weakening ENSO amplitude and the La Niña–like mean-state response are forced by global warming (see Figs. 8 and 9). Interestingly, the historical and RCP 8.5 runs suggest that the forced response could have become detectable as early as the late twentieth century. Of course, it is hard to determine whether this response is more realistic than those in the other CMIP5 models. Nevertheless, by using the M model (i.e., a state-of-the-art model with more realistic ENSO nonlinearity than some other models), we have made a case that the La Niña–like response to global warming *could* be a plausible outcome, or at least, that this La Niña–like forcing mechanism could compete with the other mechanisms that favor an El Niño–like warming. To the best of our knowledge, these conclusions have not been obtained by previous studies, because the results in those studies are often based on the multimodel means of the CMIP5 models, most of which do not realistically simulate the ENSO nonlinearity.

In section 5, we have first argued that three possible causal processes in greenhouse forcing, ENSO amplitude, and the mean-state zonal SST gradient can be outlined to explain the La Niña–like response in the M model (Fig. 10). The first one is the nonlinear ENSO warming suppression (NEWS) process, where the greenhouse forcing weakens the ENSO amplitude, which in turn cause the mean state to be La Niña–like (see also Kohyama and Hartmann 2017). The second one is the ''ENSO responds to mean state'' (ERMS) process, where the greenhouse forcing changes the mean state first, causing the ENSO amplitude change. The third is the ''ENSO independent of mean state'' (EIMS) process, in which the ENSO amplitude and the mean state are independently forced by greenhouse warming. Considering the reasonably high correlation between the ENSO amplitude and the mean-state zonal SST gradient, however, the EIMS process might be the least important process of the three.

Then, comparing the two GFDL models whose difference is only the oceanic components, we have discussed some potential physical mechanisms that can simulate the NEWS and ERMS processes in the M model. The most important difference appears to be the upper ocean thermal stratification. The stronger thermal stratification and the shallower mixed layer depth of the M model, both of which are more realistic than those of the G model at least in the historical period, might be the key to explain the realistic nonlinearity in the M model. Because the equatorial properties related to vertical diffusivities are known to be reasonably different in these models, it may be interesting to design some experiments to check the sensitivity of the ENSO nonlinearity to the background diffusivity. To understand the nature of the ENSO nonlinearity is important to evaluate the possibility of the NEWS process. From a more global perspective, on the other hand, the weaker polar amplification in the M model might be related to the origin of the anomalously cold equatorial upwelling water. This oceanic teleconnection mechanism is a possible mechanism to realize the ERMS process.

One important caveat of this study is that, to focus on the oceanic difference between the M and G model, we have only used three models to do the analyses for this study. Therefore, we have not discussed any potentially

important difference in the atmospheric components of the models. To simulate the La Niña–like trend, however, it is virtually certain that the role of the atmosphere is as important as the role of the ocean. For instance, the strength of atmospheric damping feedback (i.e., SST in a warmer climate yields stronger atmospheric damping, such as latent heat release and radiation, which leads to smaller SST variance) could have an important influence on the trends of the ENSO amplitude. In addition, the M model is not the only one model reproducing a realistic ENSO skewness (Sun et al. 2016), although it is close to the best. In particular, we have shown in Fig. 8 of Kohyama and Hartmann (2017) that the MIROC5 model exhibits the most realistic ENSO skewness among 32 CMIP5 models, and puzzlingly, that this model exhibits a strong El Niño–like mean-state warming (see also Huang and Ying 2015). Close investigations of MIROC5 might help us understand the necessary conditions of a La Niña–like mean-state warming further, although we believe it is beyond the scope of this particular study.

Some recent studies also suggest a possible relationship between the simulated historical mean-state SST and the projected mean-state SST changes (Huang and Ying 2015; Li et al. 2016; Ying and Huang 2016), particularly a linkage between the climatological SST bias and the La Niña–like mean-state warming. For instance, Huang and Ying (2015) showed by a multimodel statistical analysis that a warm bias of climatological SST in the southeastern Pacific is significantly correlated with a relatively slow warming in the southeastern Pacific, yielding a La Niña–like warming pattern. The M model exhibits the typical bias pattern found in many GCMs (Zheng et al. 2011), especially the warm bias in the southeastern Pacific and the excessive cold tongue in the western and central Pacific, to which the La Niña–like warming in this model may be attributable. This notion also appears to be consistent with the evidence that the M model exhibits more prominent warm bias in the southeastern Pacific than the G model, although the argument remains speculative without further analyses, comparison, and their physical interpretations.

The La Niña–like response and strengthened Walker circulation in the M model could also be contributed to by some other mechanisms that involve regions outside of the Pacific basin. For instance, some recent studies have suggested that the excessive warming in the tropical Indian and Atlantic Ocean relative to the tropical Pacific Ocean may enhance the Pacific trade winds in recent decades (Luo et al. 2012; McGregor et al. 2014; Zhang and Karnauskas 2016). In fact, considering that the interbasin warming contrast is more prominent in the M model than the G model (Fig. 12a), this contrast could potentially play a role to explain the difference in the Pacific response. Nevertheless, the response of atmospheric vertical motion to global warming (Fig. 3b) does not suggest any major differences over the tropical Atlantic between the two GFDL models, whereas McGregor et al. (2014) showed using a different model that a strong signal over the Atlantic is required for the mechanism to operate. This evidence does not support the notion that the Atlantic–Pacific contrast is a major contributor to the model difference, at the very least, between the two GFDL models. On the other hand, in Fig. 3b some discrepancies in the response of the tropical Indian Ocean between the two models are detectable, so the Indian–Pacific contrast could be of more importance. More comprehensive analyses using other models are required to estimate the importance of this mechanism in the real world relative to the hypotheses proposed in this study.

Preliminary analyses suggest that many other CMIP5 models do not reproduce realistic ENSO nonlinearity and therefore do not exhibit the fundamental relationship between the zonal SST gradient and the ENSO amplitude as observed in the real world. It is true that the vast majority of the CMIP5 models and the multimodel mean exhibit El Niño–like responses to global warming, but the range of spatial patterns they produce is not consistent. Hence, we do not have a lot of faith in the multimodel mean pattern of the mean-state SST warming. Considering that it is a challenging scientific problem and is important for society, further studies on the possibility of a La Niña–like response are needed.

Acknowledgments. The work was supported by the National Science Foundation (NSF) under Grant AGS-1549579, and Takenaka Scholarship Foundation. We thank Casey Wall for reading the manuscript, and Alyssa Atwood for preprocessing the output from 4000-yr-long preindustrial control run of GFDL CM2.1. We are also grateful to Cecilia Bitz, Christopher Bretherton, Matthew Harrison, Isaac Held, Andrew Shao, and two anonymous reviewers for their helpful comments and suggestions.

REFERENCES

An, S.-I., and F.-F. Jin, 2004: Nonlinearity and asymmetry of ENSO. *J. Climate*, **17**, 2399–2412, doi:10.1175/1520-0442(2004)017<2399:NAAOE>2.0.CO;2.

——, Y.-G. Ham, J.-S. Kug, F.-F. Jin, and I.-S. Kang, 2005: El Niño–La Niña asymmetry in the Coupled Model Intercomparison Project simulations. *J. Climate*, **18**, 2617–2627, doi:10.1175/JCLI3433.1.

——, J.-W. Kim, S.-H. Im, B.-M. Kim, and J.-H. Park, 2012: Recent and future sea surface temperature trends in tropical Pacific warm pool and cold tongue regions. *Climate Dyn.*, **39**, 1373–1383, doi:10.1007/s00382-011-1129-7.

Andrews, T., J. M. Gregory, M. J. Webb, and K. E. Taylor, 2012: Forcing, feedbacks and climate sensitivity in CMIP5 coupled

atmosphere–ocean climate models. *Geophys. Res. Lett.*, **39**, L09712, doi:10.1029/2012GL051607.

Atwood, A. R., D. S. Battisti, A. T. Wittenberg, W. H. G. Roberts, and D. J. Vimont, 2017: Characterizing unforced multi-decadal variability of ENSO: A case study with the GFDL CM2.1 coupled GCM. *Climate Dyn.*, doi:10.1007/s00382-016-3477-9, in press.

Battisti, D. S., and A. C. Hirst, 1989: Interannual variability in a tropical atmosphere–ocean model: Influence of the basic state, ocean geometry and nonlinearity. *J. Atmos. Sci.*, **46**, 1687–1712, doi:10.1175/1520-0469(1989)046<1687:IVIATA>2.0.CO;2.

Behringer, D., and Y. Xue, 2004: Evaluation of the global ocean data assimilation system at NCEP: The Pacific Ocean. *Proc. Eighth Symp. on Integrated Observing and Assimilation Systems for Atmosphere, Oceans, and Land Surface*, Seattle, WA, Amer. Meteor. Soc., 2.3. [Available online at https://ams.confex.com/ams/84Annual/techprogram/paper_70720.htm.]

Bellenger, H., É. Guilyardi, J. Leloup, M. Lengaigne, and J. Vialard, 2014: ENSO representation in climate models: From CMIP3 to CMIP5. *Climate Dyn.*, **42**, 1999–2018, doi:10.1007/s00382-013-1783-z.

Bretherton, C. S., M. Widmann, V. P. Dymnikov, J. M. Wallace, and I. Bladé, 1999: The effective number of spatial degrees of freedom of a time-varying field. *J. Climate*, **12**, 1990–2009, doi:10.1175/1520-0442(1999)012<1990:TENOSD>2.0.CO;2.

Cane, M. A., A. C. Clement, A. Kaplan, Y. Kushnir, D. Pozdnyakov, R. Seager, S. E. Zebiak, and R. Murtugudde, 1997: Twentieth-century sea surface temperature trends. *Science*, **275**, 957–960, doi:10.1126/science.275.5302.957.

Christensen, J., and Coauthors, 2013: Climate phenomena and their relevance for future regional climate change. *Climate Change 2013: The Physical Science Basis*, Cambridge University Press, 1217–1308, doi:10.1017/CBO9781107415324.028.

Clement, A. C., R. Seager, M. A. Cane, and S. E. Zebiak, 1996: An ocean dynamical thermostat. *J. Climate*, **9**, 2190–2196, doi:10.1175/1520-0442(1996)009<2190:AODT>2.0.CO;2.

Collins, M., and Coauthors, 2005: El Niño– or La Niña–like climate change? *Climate Dyn.*, **24**, 89–104, doi:10.1007/s00382-004-0478-x.

——, and Coauthors, 2010: The impact of global warming on the tropical Pacific Ocean and El Niño. *Nat. Geosci.*, **3**, 391–397, doi:10.1038/ngeo868.

Dee, D. P., and Coauthors., 2011: The ERA-interim reanalysis: Configuration and performance of the data assimilation system. *Quart. J. Roy. Meteor. Soc.*, **137**, 553–597, doi:10.1002/qj.828.

Delworth, T. L., and Coauthors, 2006: GFDL's CM2 global coupled climate models. Part I: Formulation and simulation characteristics. *J. Climate*, **19**, 643–674, doi:10.1175/JCLI3629.1.

DiNezio, P. N., A. C. Clement, G. A. Vecchi, B. J. Soden, B. P. Kirtman, and S.-K. Lee, 2009: Climate response of the equatorial Pacific to global warming. *J. Climate*, **22**, 4873–4892, doi:10.1175/2009JCLI2982.1.

Dunne, J. P., and Coauthors, 2012: GFDL's ESM2 global coupled climate–carbon Earth system models. Part I: Physical formulation and baseline simulation characteristics. *J. Climate*, **25**, 6646–6665, doi:10.1175/JCLI-D-11-00560.1.

——, and Coauthors, 2013: GFDL's ESM2 global coupled climate–carbon Earth system models. Part II: Carbon system formulation and baseline simulation characteristics. *J. Climate*, **26**, 2247–2267, doi:10.1175/JCLI-D-12-00150.1.

Goodman, P. J., W. Hazeleger, P. de Vries, and M. Cane, 2005: Pathways into the Pacific Equatorial Undercurrent: A trajectory analysis. *J. Phys. Oceanogr.*, **35**, 2134–2151, doi:10.1175/JPO2825.1.

Harrison, M., and R. Hallberg, 2008: Pacific subtropical cell response to reduced equatorial dissipation. *J. Phys. Oceanogr.*, **38**, 1894–1912, doi:10.1175/2008JPO3708.1.

Held, I. M., and B. J. Soden, 2006: Robust responses of the hydrological cycle to global warming. *J. Climate*, **19**, 5686–5699, doi:10.1175/JCLI3990.1.

——, M. Winton, K. Takahashi, T. Delworth, F. Zeng, and G. K. Vallis, 2010: Probing the fast and slow components of global warming by returning abruptly to preindustrial forcing. *J. Climate*, **23**, 2418–2427, doi:10.1175/2009JCLI3466.1.

Huang, P., and J. Ying, 2015: A multimodel ensemble pattern regression method to correct the tropical Pacific SST change patterns under global warming. *J. Climate*, **28**, 4706–4723, doi:10.1175/JCLI-D-14-00833.1.

Jin, F.-F., S.-I. An, A. Timmermann, and J. Zhao, 2003: Strong El Niño events and nonlinear dynamical heating. *Geophys. Res. Lett.*, **30**, 1120, doi:10.1029/2002GL016356.

Knutson, T. R., and S. Manabe, 1995: Time-mean response over the tropical Pacific to increased CO_2 in a coupled ocean–atmosphere model. *J. Climate*, **8**, 2181–2199, doi:10.1175/1520-0442(1995)008<2181:TMROTT>2.0.CO;2.

Kohyama, T., and D. L. Hartmann, 2016: Antarctic sea ice response to weather and climate modes of variability. *J. Climate*, **29**, 721–741, doi:10.1175/JCLI-D-15-0301.1.

——, and ——, 2017: Nonlinear ENSO warming suppression (NEWS). *J. Climate*, **30**, 4227–4251, doi:10.1175/JCLI-D-16-0541.1.

L'Heureux, M. L., S. Lee, and B. Lyon, 2013: Recent multidecadal strengthening of the Walker circulation across the tropical Pacific. *Nat. Climate Change*, **3**, 571–576, doi:10.1038/nclimate1840.

Li, G., S.-P. Xie, Y. Du, and Y. Luo, 2016: Effects of excessive equatorial cold tongue bias on the projections of tropical Pacific climate change. Part I: The warming pattern in CMIP5 multi-model ensemble. *Climate Dyn.*, **47**, 3817–3831, doi:10.1007/s00382-016-3043-5.

Luo, J.-J., W. Sasaki, and Y. Masumoto, 2012: Indian Ocean warming modulates Pacific climate change. *Proc. Natl. Acad. Sci. USA*, **109**, 18 701–18 706, doi:10.1073/pnas.1210239109.

McGregor, S., A. Timmermann, M. F. Stuecker, M. H. England, M. Merrifield, F.-F. Jin, and Y. Chikamoto, 2014: Recent Walker circulation strengthening and Pacific cooling amplified by Atlantic warming. *Nat. Climate Change*, **4**, 888–892, doi:10.1038/nclimate2330.

Meinshausen, M., and Coauthors, 2011: The RCP greenhouse gas concentrations and their extensions from 1765 to 2300. *Climatic Change*, **109**, 213–241, doi:10.1007/s10584-011-0156-z.

Meng, Q., M. Latif, W. Park, N. S. Keenlyside, V. A. Semenov, and T. Martin, 2012: Twentieth century Walker circulation change: Data analysis and model experiments. *Climate Dyn.*, **38**, 1757–1773, doi:10.1007/s00382-011-1047-8.

Murakami, H., R. Mizuta, and E. Shindo, 2012: Future changes in tropical cyclone activity projected by multi-physics and multi-SST ensemble experiments using the 60-km-mesh MRI-AGCM. *Climate Dyn.*, **39**, 2569–2584, doi:10.1007/s00382-011-1223-x.

Rayner, N., D. E. Parker, E. Horton, C. Folland, L. Alexander, D. Rowell, E. Kent, and A. Kaplan, 2003: Global analyses of sea surface temperature, sea ice, and night marine air temperature since the late nineteenth century. *J. Geophys. Res.*, **108** (D14), 4407, doi:10.1029/2002JD002670.

Rodgers, K. B., B. Blanke, G. Madec, O. Aumont, P. Ciais, and J.-C. Dutay, 2003: Extratropical sources of equatorial Pacific upwelling in an OGCM. *Geophys. Res. Lett.*, **30**, 1084, doi:10.1029/2002GL016003.

Seager, R., and R. Murtugudde, 1997: Ocean dynamics, thermocline adjustment, and regulation of tropical SST. *J. Climate*, **10**, 521–534, doi:10.1175/1520-0442(1997)010<0521:ODTAAR>2.0.CO;2.

Smith, T. M., R. W. Reynolds, T. C. Peterson, and J. Lawrimore, 2008: Improvements to NOAA's historical merged land–ocean surface temperature analysis (1880–2006). *J. Climate*, **21**, 2283–2296, doi:10.1175/2007JCLI2100.1.

Sun, Y., F. Wang, and D.-Z. Sun, 2016: Weak ENSO asymmetry due to weak nonlinear air–sea interaction in CMIP5 climate models. *Adv. Atmos. Sci.*, **33**, 352–364, doi:10.1007/s00376-015-5018-6.

Tanaka, H. L., N. Ishizaki, and D. Nohara, 2005: Intercomparison of the intensities and trends of Hadley, Walker and monsoon circulations in the global warming projections. *Sci. Online Lett. Atmos.*, **1**, 77–80, doi:10.2151/sola.2005-021.

Taylor, K. E., R. J. Stouffer, and G. A. Meehl, 2012: An overview of CMIP5 and the experiment design. *Bull. Amer. Meteor. Soc.*, **93**, 485–498, doi:10.1175/BAMS-D-11-00094.1.

Tokinaga, H., S.-P. Xie, C. Deser, Y. Kosaka, and Y. M. Okumura, 2012a: Slowdown of the Walker circulation driven by tropical Indo-Pacific warming. *Nature*, **491**, 439–443, doi:10.1038/nature11576.

——, ——, A. Timmermann, S. McGregor, T. Ogata, H. Kubota, and Y. M. Okumura, 2012b: Regional patterns of tropical Indo-Pacific climate change: Evidence of the Walker circulation weakening. *J. Climate*, **25**, 1689–1710, doi:10.1175/JCLI-D-11-00263.1.

Tsuchiya, M., R. Lukas, R. A. Fine, E. Firing, and E. Lindstrom, 1989: Source waters of the Pacific Equatorial Undercurrent. *Prog. Oceanogr.*, **23**, 101–147, doi:10.1016/0079-6611(89)90012-8.

Vecchi, G. A., and B. J. Soden, 2007: Global warming and the weakening of the tropical circulation. *J. Climate*, **20**, 4316–4340, doi:10.1175/JCLI4258.1.

——, ——, A. T. Wittenberg, I. M. Held, A. Leetmaa, and M. J. Harrison, 2006: Weakening of tropical Pacific atmospheric circulation due to anthropogenic forcing. *Nature*, **441**, 73–76, doi:10.1038/nature04744.

Wittenberg, A. T., A. Rosati, N.-C. Lau, and J. J. Ploshay, 2006: GFDL's CM2 global coupled climate models. Part III: Tropical Pacific climate and ENSO. *J. Climate*, **19**, 698–722, doi:10.1175/JCLI3631.1.

Xiang, B., B. Wang, J. Li, M. Zhao, and J.-Y. Lee, 2014: Understanding the anthropogenically forced change of equatorial Pacific trade winds in coupled climate models. *J. Climate*, **27**, 8510–8526, doi:10.1175/JCLI-D-14-00115.1.

Xie, S.-P., C. Deser, G. A. Vecchi, J. Ma, H. Teng, and A. T. Wittenberg, 2010: Global warming pattern formation: Sea surface temperature and rainfall. *J. Climate*, **23**, 966–986, doi:10.1175/2009JCLI3329.1.

Ying, J., and P. Huang, 2016: Cloud–radiation feedback as a leading source of uncertainty in the tropical Pacific SST warming pattern in CMIP5 models. *J. Climate*, **29**, 3867–3881, doi:10.1175/JCLI-D-15-0796.1.

——, ——, and R. Huang, 2016: Evaluating the formation mechanisms of the equatorial Pacific SST warming pattern in CMIP5 models. *Adv. Atmos. Sci.*, **33**, 433–441, doi:10.1007/s00376-015-5184-6.

Yokoi, S., and Y. N. Takayabu, 2009: Multi-model projection of global warming impact on tropical cyclone genesis frequency over the western North Pacific. *J. Meteor. Soc. Japan*, **87**, 525–538, doi:10.2151/jmsj.87.525.

Zebiak, S. E., and M. A. Cane, 1987: A model El Niño–Southern Oscillation. *Mon. Wea. Rev.*, **115**, 2262–2278, doi:10.1175/1520-0493(1987)115<2262:AMENO>2.0.CO;2.

Zhang, L., and K. B. Karnauskas, 2016: The role of tropical interbasin SST gradients in forcing Walker circulation trends. *J. Climate*, **30**, 499–508, doi:10.1175/JCLI-D-16-0349.1.

Zhang, M., and H. Song, 2006: Evidence of deceleration of atmospheric vertical overturning circulation over the tropical Pacific. *Geophys. Res. Lett.*, **33**, L12701, doi:10.1029/2006GL025942.

Zheng, X.-T., S.-P. Xie, L.-H. Lv, and Z.-Q. Zhou, 2016: Inter-model uncertainty in ENSO amplitude change tied to Pacific Ocean warming pattern. *J. Climate*, **29**, 7265–7279, doi:10.1175/JCLI-D-16-0039.1.

Zheng, Y., T. Shinoda, J.-L. Lin, and G. N. Kiladis, 2011: Sea surface temperature biases under the stratus cloud deck in the southeast Pacific Ocean in 19 IPCC AR4 coupled general circulation models. *J. Climate*, **24**, 4139–4164, doi:10.1175/2011JCLI4172.1.